ARTICLE

Controllable Growth of Nanoscale Conductive Filaments in Solid-Electrolyte-Based ReRAM by Using a Metal Nanocrystal Covered Bottom Electrode

Qi Liu,[†,‡] Shibing Long,[†] Hangbing Lv,[†] Wei Wang,[†,§] Jiebin Niu,[†] Zongliang Huo,[†] Junning Chen,[‡] and Ming Liu[†,*]

[†]Laboratory of Nano-Fabrication and Novel Devices Integrated Technology, Institute of Microelectronics, Chinese Academy of Sciences, Beijing 100029, China, [‡]College of Electronics and Technology, Anhui University, Hefei 230039, China, and [§]College of Nanoscale Science and Engineering (CNSE), University at Albany, New York 12203

ABSTRACT Resistive memory (ReRAM) based on a solid-electrolyte insulator is a promising nanoscale device and has great potentials in nonvolatile memory, analog circuits, and neuromorphic applications. The underlying resistive switching (RS) mechanism of ReRAM is suggested to be the formation and rupture of nanoscale conductive filament (CF) inside the solid-electrolyte layer. However, the random nature of the nucleation and growth of the CF makes their formation difficult to control, which is a major obstacle for ReRAM performance improvement. Here, we report a novel approach to resolve this challenge by adopting a metal nanocrystal (NC) covered bottom electrode (BE) to replace the conventional ReRAM BE. As a demonstration vehicle, a Ag/ZrO_2/Cu NC/Pt structure is prepared and the Cu NC covered Pt BE can control CF nucleation and growth to provide superior uniformity of RS properties. The controllable growth of nanoscale CF bridges between Cu NC and Ag top electrode has been vividly observed by transmission electron microscopy (TEM). On the basis of energy-dispersive X-ray spectroscopy (EDS) and elemental mapping analyses, we further confirm that the chemical contents of the CF are mainly Ag atoms. These testing/metrology results are consistent with the simulation results of electric-field distribution, showing that the electric field will enhance and concentrate on the NC sites and control location and orientation of Ag CFs.

KEYWORDS: resistive switching · nonvolatile memory · solid electrolyte · ZrO_2 · conductive filament · metal nanocrystal

*Address correspondence to liuming@ime.ac.cn.

Received for review July 24, 2010 and accepted September 10, 2010.

Published online September 20, 2010.
10.1021/nn1017582

© 2010 American Chemical Society

Current nonvolatile memory technology, such as flash, is based on charge storage and is rapidly reaching its physical limits.[1] Therefore, non-charge-based nanoscale memory devices are being intensively studied for next generation nonvolatile memory applications, such as magnetic random access memory (MRAM),[2] phase-change random access memory (PcRAM),[3] and resistive random access memory (ReRAM).[4,5] Among all of the emerging technologies, the ReRAM nanodevice is one of the most promising candidates, due to its simple structure, high density, low power, and excellent scalability.[4−8] More importantly, some ReRAM devices based on mixed ions/electron conductors are demonstrated with a particular resistive switching behavior such that their resistance can be incrementally modified by controlling charge or flux through it.[9−11] This behavior is similar to the memristor operation (the fourth fundamental passive circuit element in addition to resistor, capacitor, and inductor).[12] The memristive characteristics might expand the use of ReRAM devices from memory to many emerging applications such as analog and neuromorphic ICs.[13−15]

The solid-electrolyte insulator is one of the mixed conductors, and it has been extensively studied as functional material of the ReRAM.[14−19] Generally, the solid-electrolyte insulator sandwiches between an oxidizable electrode (Cu or Ag) and an inert (Pt or W) electrode to form a solid-electrolyte-based ReRAM device, also known as conductive bridging RAM (CBRAM)[6] or a programmable metallization cell (PMC).[16] The resistance of the ReRAM device can switch between high resistive state (HRS or OFF-state) and low resistive state (LRS or ON-state) under electrical spurring because the diffusion of metal ions (*i.e.*, Cu^+ or Ag^+) and their oxidation/reduction reactions can be formation/rupture of the nanoscale conductive filament (CF) inside the solid-electrolyte layer.[17,18] Individual solid-electrolyte-based ReRAM devices have demonstrated high cycling stability ($>10^8$), data retention times in excess of one year, large R_{ON}/R_{OFF} ratio of ($>10^7$), sub-1 V operation voltages, GHz

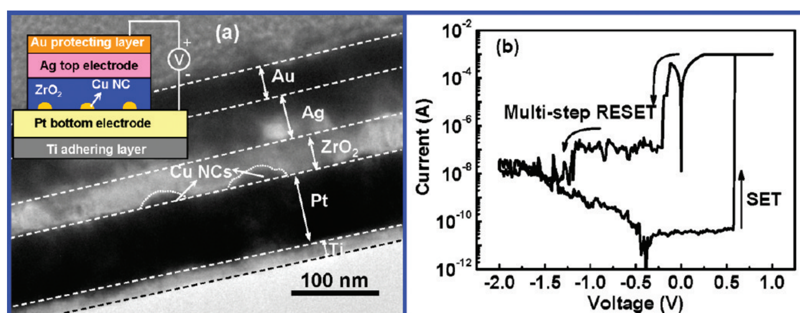

Figure 1. (a) Cross-section TEM image for the Ag/ZrO_2/Cu NC/Pt memory device. The Cu NC layer is stacked on the surface of the Pt BE layer. The inset shows a schematic configuration of the device structure. (b) Typical $I-V$ curves of the Ag/ZrO_2/Cu NC/Pt memory device with an area of 500 × 500 nm^2 under DC voltage sweep mode.

switching speeds, and switching currents in the nanoampere range.[6,17,19] However, the devices often show large variation of switching voltages and resistance states due to the random nature of the nucleation/growth of the CF. The random nature characteristics make CF difficult to form along with the same path in repetitive switching cycles.[4,17] In order to improve the device uniformity, previous studies focused primarily on materials improvement, including optimization of the crystallographic structure[20]/stoichiometry[21] of the oxide materials, adaptation of the active bottom/top electrode materials,[22] or impurity doping of oxide materials.[23,24] On the other hand, none of these approaches is aimed to directly address the fundamental challenge, such as controlling the location and orientation of the CF growth and rupture.

In this work, by inserting a metallic nanocrystal (NC) layer between the inert bottom electrode and the solid-electrolyte layer of a Ag/ZrO_2/Cu NC/Pt ReRAM device, we have been able to manipulate the location and orientation of the controlled CF as observed directly by TEM. This controlled CF growth method not only serves to reduce the randomness of the CF growth process and improve the device performance but also enables a deeper understanding of the microscopic mechanisms of the CF formation process.

RESULTS AND DISCUSSION

The Ag/ZrO_2/Cu NC/Pt structure consists of a Ag top electrode (TE) layer, an active ZrO_2 layer, and a Cu NC/Pt-stacked layer as the bottom electrode (BE), which is schematically shown in the inset of Figure 1a. The cross-sectional TEM image of a Ag/ZrO_2/Cu NC/Pt memory cell in Figure 1a clearly shows Cu NCs embedded in the ~40 nm thick ZrO_2 layer at the interface with the Pt BE. Figure 1b shows a typical current−voltage ($I-V$) curve of a 500 × 500 nm^2 Ag/ZrO_2/Cu NC/Pt memory cell. The as-deposited devices are normally in the OFF-state (resistance $>10^9$ Ω) and do not require an electroforming process to induce the RS. When a positive voltage applied to the Ag TE exceeds the SET voltage (V_{SET}), the current of the device rapidly increases and the device transits from the OFF-state to the ON-state. In this SET process, the current compliance is limited by 1 mA to avoid device failure caused by high leakage. Subsequently, upon sweeping the applied voltage in the negative direction (0 V → −2 V), the device suddenly transits back to the OFF-state at a RESET voltage (V_{RESET}). It is worthwhile to note that a stepwise RESET process is frequently observed in this memory device, implying that the switching behavior is dominated by formation and annihilation of multiple CFs.[17] The typical resistances of the ON-state and the OFF-state (on the order of 10^2 and 10^9 Ω, respectively) are obtained using the 0.05 V read voltage. With a R_{OFF}/R_{ON} ratio of more than 10^7, the memory device has an ultrahigh operation window for efficient memory applications.

To verify that the growth of the CFs is controlled by the metallic NCs, a TEM was used to directly capture the CF growth process in the Ag/ZrO_2/Cu NC/Pt memory cell. First, a 10 × 10 μm^2 memory cell was set to the ON-state (R_{ON} ~ 200 Ω) through three repetitive switching cycles (which concluded at the SET operation). At this point, a site-specific *in situ* lift-out method was carried out using a dual-beam focused ion beam (FIB) to prepare a ~100 nm thick TEM specimen (SET sample). Figure 2a shows a cross-sectional TEM image of the SET sample. A dark, nanometer-sized region (as marked by the red square) can be seen to bridge the Ag TE and the Pt BE across the ZrO_2 layer. This "nanobridge" region is directly connected to a protrusion of the Pt BE, which is identified as a Cu NC using EDS (right-most region in the relative atomic concentration plot in Figure 2d). This confirms that the CF growth is directed to the metal NC. Figure 2b shows a magnified TEM image of the red square region in Figure 2a. The shape of the nanobridge region is nearly cylindrical, which is consistent with the prediction that the shape of CF is generally cylindrical in solid-electrolyte-based ReRAM.[25] This cylindrical CF is the typical one among the three connected CFs observed in the TEM sample under high angle annular dark field (HAADF) imaging in scanning TEM (STEM) mode. This further confirms that the switching phenomena of such devices are dominated by formation and annihilation of multiple CFs.

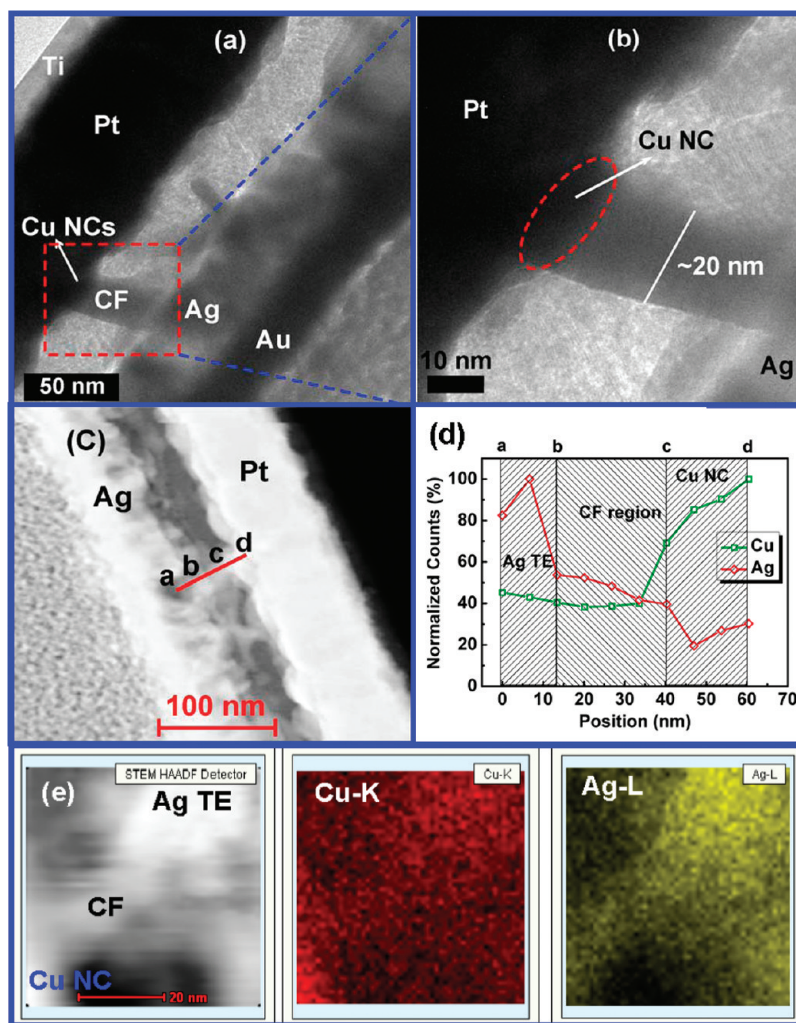

Figure 2. TEM and EDS investigation of the sample in SET state. (a) Low-magnification cross-section TEM image of the Ag/ZrO_2/Cu NC/Pt memory cell after SET process. The image shows possible CF regions. (b) Enlarged images of the red square regions in (a). (c) STEM-HAADF image of the device. (d) Line profile of the EDS intensity of Ag and Cu elements along the red line in (c). The results show that the nanobridge region is directly connected to the Cu NC. (e) EDS elemental mapping images of Cu and Ag elements across the nanobridge region. This indicates that the CF mainly consists of Ag.

The chemical composition of one of these nanobridge regions was characterized by HAADF imaging and EDS compositional analysis in STEM mode. As shown in Figure 2c, the nanobridge has a high relative contrast in the STEM-HAADF image, similar to the Ag TE and the Pt BE regions. This indicates that it is composed primarily of high-*Z* elements. Further chemical analysis along the nanobridge axis was carried out *via* EDS profiling (marked as red line). On the basis of the change of the relative Ag and Cu atomic concentrations across the nanobridge region, the EDS profile can be divided into three distinct sections, as shown in Figure 2d: (i) a→b corresponds to the Ag electrode region; (ii) b→c corresponds to the CF region; and (iii) c→d corresponds to the Cu NC region. The result demonstrated that this nanobridge region is directly connected to the Cu NC. Note that the EDS intensity associated with elemental Cu includes a contribution from the Cu TEM grid supporting the device sample. Thus, it cannot be determined whether the Cu is a major compositional component of the CF or Ag element in the b→c and a→b regions, respectively. To further analyze the composition of the CF, an EDS elemental mapping was carried out in STEM mode. The STEM elemental images reveal a uniform distribution of Cu across the region (Figure 2e). This is in contrast to the Ag distribution, which is more concentrated in the nanobridge region (Figure 2e), and suggests that Ag is the primary elemental component of the nanobridge CF in our Ag/ZrO_2/Cu NC/Pt memory device.

The rupture process of the CFs in the Ag/ZrO_2/Cu NC/Pt memory device was studied by TEM using samples in the RESET state. Before preparing the RESET samples for TEM observation, two 10 × 10 μm^2 memory cells were set to the OFF-state ($R_{OFF} \sim 10^9\ \Omega$) through three repetitive switching cycles (the final operation consists of the RESET process). In the 4 μm effective observation width, no obvious connected or dis-

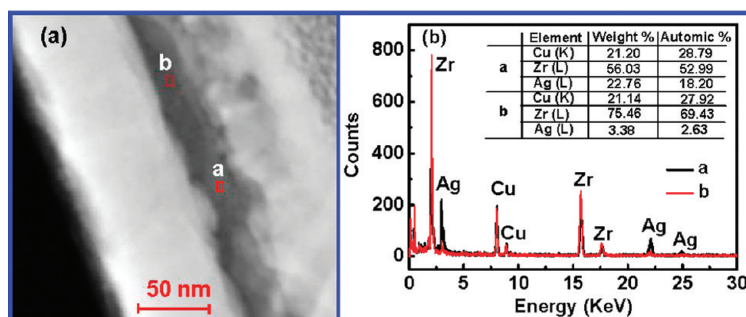

	Element	Weight %	Automic %
a	Cu (K)	21.20	28.79
	Zr (L)	56.03	52.99
	Ag (L)	22.76	18.20
b	Cu (K)	21.14	27.92
	Zr (L)	75.46	69.43
	Ag (L)	3.38	2.63

Figure 3. TEM and EDS investigation of sample in RESET state. (a) STEM-HAADF image of the RESET sample, in which the regions for EDS analyses are denoted by red square. (b) EDS spectrum collected from the square region "a" above the Cu NC and the region "b" without Cu NC. The intensity of Ag, Zr, and Cu elements collected from both regions are shown in the inset table.

connected CF is observed in either RESET samples (Figure 3a). This TEM result indicates that the Ag CFs might dissolve completely after the RESET process, consistent with the experimental observation that the resistance of the Ag/ZrO_2/Cu NC/Pt memory device in the OFF-state is almost equal to the resistance of the initial state.[26] To investigate this further, the chemical composition of the ZrO_2 film in the different regions was also studied *via* EDS analysis. As shown in Figure 3b, the Ag element concentration in the ZrO_2 film above the Cu NC (square region labeled "a" in Figure 3a) is much larger than in the region without Cu NC (square region labeled "b" in Figure 3a). Although the EDS results cannot be used to directly prove the prior existence of a CF in the "a" region, the high Ag concentration in the "a" region is consistent with CF formation and rupture during repetitive RS operation.

The observed NC-controlled Ag CF growth in our device can be explained by electric-enhanced, redox-based ion-migration mechanism. On the basis of the electrochemical metallization theory,[27] the Ag CF growth process can be divided into three portions: (i) oxidation of Ag atoms to Ag^+ ions in the Ag anode (Ag $\rightarrow Ag^+ + e^-$); (ii) drift of Ag^+ cations toward the Pt cathode under the electric field; (iii) deoxidation of Ag^+ cations back to Ag atoms ($Ag^+ + e^- \rightarrow Ag$) followed by Ag cluster nucleation and growth on the surface of the cathode. The randomness of the CF growth process is likely the result from the stochastic characteristics of the nucleation phenomena.[27] In the CF growth process, the electromigration of Ag^+ cations is closely associated with the electric-field strength inside the ZrO_2 matrix, and the Ag^+ ionic current density can be depicted by Mott and Gurney's eq 1:[27]

$$i = 2qcav\exp\left(-\frac{W_a^0}{kT}\right)\sin h\left(\frac{aqE}{2kT}\right) \qquad (1)$$

where c is the concentration of mobile cations, a is the jump distance of the ions (a generally is equal to several nanometers),[27] v is a frequency factor, W_a is the energy barrier for ion hopping, E is electric field, k is Boltzmann's constant, and T is the absolute temperature.

From eq 1, the ionic current density displays an exponential dependence on E in the high electric field ($aqE \gg 2kT$) condition. To study the impact of the Cu NC on the electric field, we systematically investigate the electric-field distribution in the ZrO_2 layer by using Matlab PDE tool and TCAD. The detail of the simulation is provided in the Supporting Information. The simulation results demonstrate that electric-field lines converge around the NC site (Supporting Figure S1), and the intensity of the electric field at the tip of NC can greatly exceed that of the planar region (Supporting Figures S2 and S3). Due to the NC-enhanced electric field, more Ag^+ ions converge around the NC location than other regions of the Pt surface, which greatly increases the nucleation probability of Ag atoms at the NC sites.[26] Once the Ag nucleus is formed, the tip of the Ag nucleus will have the highest electrochemical deposition rate of Ag atoms due to high electric field.[25] This promotes the growth of the Ag CF to the TE and forms a highly conductive path through the ZrO_2.

In contrast, when the polarity of the applied voltage is reversed, the device will switch back to the OFF-state due to the dissolution or rupture of the Ag CFs resulting from a reversed electrochemical reaction[28] or thermally assisted electrochemical reaction.[29] It is noteworthy that a large number of Ag elements in the ZrO_2 layer above the NC remain after the RESET process (Figure 3a), which could serve to promote CF formation during the subsequent SET process. Thus, on the basis of the NC-enhanced electrical field analysis, we suggest that CFs are easily formed, ruptured, and re-formed along the same paths in repetitive switching cycles. This process can be used to substantially improve the uniformity of the CF-based ReRAM.

If the proposed CF formation/reformation mechanism applies, the Ag/ZrO_2/Cu NC/Pt memory device is expected to exhibit stability and uniformity with respect to its RS behaviors. Figure 4a shows the $I-V$ curves for 20 continuous RS cycles of a Ag/ZrO_2/Cu NC/Pt memory cell. Indeed, the Ag/ZrO_2/Cu NC/Pt memory device exhibits excellent stability in its RS behavior and a very narrow

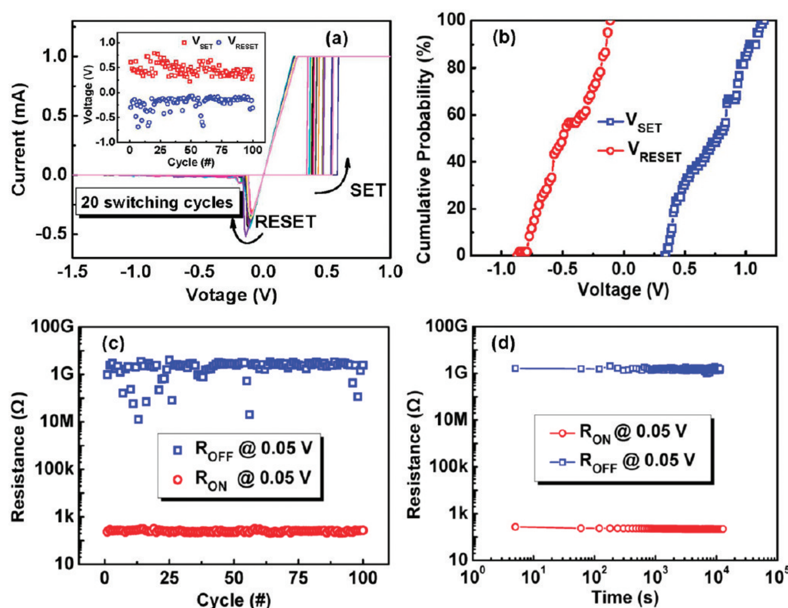

Figure 4. (a) Reproducibility of resistive switching (20 cycles) in voltage sweeping mode (0 V → 1 V → 0 V → −2 V → 0 V) of the Ag/ZrO_2/Cu NC/Pt memory device with a 500 × 500 nm^2 cell area. The inset shows the values of SET and RESET voltages for a Ag/ZrO_2/Cu NC/Pt memory cell under 100-time continuous switching cycles. (b) Cell to cell cumulative distribution of the SET and RESET voltages in Ag/ZrO_2/Cu NC/Pt memory devices. These results are statistical data from 50 RS cycles for five cells with an area of 500 × 500 nm^2. (c) Endurance test of the Ag/ZrO_2/Cu NC/Pt memory device under DC switching sweep mode (0 V → 1 V → 0 V → −2 V → 0 V). (d) Retention test of the Ag/ZrO_2/Cu NC/Pt memory device under a 0.05 V continuous read voltage stress.

distribution of both SET and RESET voltages. Moreover, in a 100 continuous RS cycle test, the values of V_{SET} and V_{RESET} are confined to ranges between 0.3 and 0.8 V and between −0.15 and −0.7 V, respectively. This is shown in the inset of Figure 4a. Due to the multistep RESET process, V_{RESET} is extracted from the jump threshold voltage corresponding to a resistance larger than 10^5 Ω in the $I-V$ curves. Compared with the control sample (Ag/ZrO_2/Pt), and other traditional solid-electrolyte-based ReRAM,[24,30] the Ag/ZrO_2/Cu NC/Pt memory device shows a narrower distribution of V_{SET} for a single memory cell. The electrical characteristics of the control sample are described in the Supporting Information. Moreover, the device-to-device variations of the switching threshold voltages in the Ag/ZrO_2/Cu NC/Pt memory devices in terms of the cumulative distribution of V_{SET}/V_{RESET} for multiple memory cells under multiple RS cycles were investigated and are shown in Figure 4b. Although the device-to-device distribution ranges of V_{SET} and V_{RESET} were broadened to 0.3 to 1.2 and −0.1 to −0.8 V, respectively, the uniformity of the Ag/ZrO_2/Cu NC/Pt memory device still represents a significant improvement over that of Ag/ZrO_2/Pt device (Supporting Figure S4b) and our other previous samples without NC insertion.[17,23,31] Figure 4c shows the resistance of a Ag/ZrO_2/Cu NC/Pt memory cell in the ON- and OFF-states *versus* the number of switching cycles at 0.05 V readout voltages. It is seen that the resistance in the LRS has a narrow distribution in the range of 200−320 Ω, while the resistance of the HRS exhibits a broader range of dispersions (1×10^7 to 3×10^9 Ω). In most cases, the resistance of the OFF-state can be restored to the initial resistance value (~10^9 Ω) under 0 V → −2 V RESET voltage sweeping, implying that the CFs are completely dissolved after the RESET process. Considering the CF dissolution mechanism, we believe that the fluctuation of R_{OFF} may be improved by using a reasonably higher or a longer duration RESET voltage. The retention property of the devices for both resistance states is shown in Figure 4d. Apparently, the resistance values in both states are stable and exhibit minimal degradation over 10^4 s, confirming the nonvolatile and the nondestructive readout properties of the device.

CONCLUSIONS

In summary, we have demonstrated an effective method to control the CF growth process in the solid-electrolyte-based ReRAM by using metal NCs covering the bottom electrode. On the basis of TEM image analysis, we conclude that CFs grow easily along the direction of the metal NC, which enables their formation along the same path during repeating RS cycles. The NC-guided CF growth reduces the randomness of the CF formation and rupture processes, leading to improvement of stability and uniformity of CF-based ReRAM. This work provides a feasible way to control the CF formation path by metal NC or other electric-field-concentrating initiators. Furthermore, the size of the electric-field-concentrating initiators can be further reduced by using self-assembly[32] or grain-boundary-mediated diffusion methods,[33] leading to devices with well-controlled filament formation even at sub-10 nm scale.

METHOD

The Ag/ZrO_2/Cu NC/Pt memory device was prepared using the following processes. After the first e-beam lithography process, horizontal stripes of the Pt/Ti (80/20 nm) bottom electrode, grown by e-beam evaporation, were transferred onto the SiO_2/Si substrate through a lift-off process. Then, the second e-beam lithography process was performed to pattern the switching layer. After that, squares of 3 nm Cu thin film and 40 nm ZrO_2 function layers were successively deposited by e-beam evaporation. Following the second lift-off process, the ZrO_2/Cu/Pt/Ti stacking films were annealed at 600 °C for 5 s in a N_2 ambient environment to form discrete Cu NCs on the surface of Pt layer. Then, vertical stripes of the Ag/Au (70/30 nm) top electrode were deposited in succession using e-beam evaporation after the third e-beam lithography. The Au layer was used to avoid the oxidation of the Ag electrode during testing and to prevent the probe tip from scratching the device surfaces. Finally, the third lift-off process was used to release the Ag/ZrO_2/Cu NC/Pt memory device. We have fabricated the devices with cell areas ranging from 0.25 μm^2 (0.5 μm $\times$ 0.5 μm) to 100 μm^2 (10 μm $\times$ 10 μm). To confirm the role of Cu NC in resistive switching phenomenon, control samples (Ag/ZrO_2/Pt) were fabricated with the same process. The resistive switching behavior of the Ag/ZrO_2/Cu NC/Pt memory device and the control sample was measured at room temperature using a Keithley 4200 semiconductor characterization system. The TEM specimens were prepared by using a FIB system (FEI Nov 200). A 200 kV field emission TEM (Tecnai G2 F20 U-TWIN) was used for TEM and EDS investigation.

Acknowledgment. The authors thank Prof. Robert Geer's useful suggestions, Dr. K. W. Peng for preparing the TEM specimens, and Dr. X. Y. Qin for TEM, STEM, and EDX analyses. This work is supported by USA NSF Grant No. 0829824, the Chinese 973 Projects 2010CB934200 and 2006CB302706, the Chinese NSFC under Grant Nos. 60825403 and 50972160, and the Chinese 863 Projects 2008AA031403 and 2009AA03Z306.

Supporting Information Available: Additional discussion on the simulation of the electrical field. The resistive switching characteristics of the control sample (Ag/ZrO_2/Pt device). This material is available free of charge *via* the Internet at http://pubs.acs.org.

REFERENCES AND NOTES

1. Meijer, G. I. Who Wins the Nonvolatile Memory Race? *Science* **2008**, *319*, 1625–1626.
2. Parkin, S. S. P.; Hayashi, M.; Thomas, L. Magnetic Domain-Wall Racetrack Memory. *Science* **2008**, *320*, 190–194.
3. Wuttig, M.; Yamada, N. Phase-Change Materials for Rewriteable Data Storage. *Nat. Mater.* **2007**, *6*, 824–832.
4. Waser, R.; Aono, M. Nanoionics-Based Resistive Switching Memories. *Nat. Mater.* **2007**, *6*, 833–840.
5. Sawa, A. Resistive Switching in Transition Metal Oxides. *Mater. Today.* **2008**, *11*, 28–36.
6. Kund, M.; Beitel, G.; Pinnow, C.-U.; Röhr, T.; Schumann, J.; Symanczyk, R.; Ufert, K.-D.; Müller, G. Conductive Bridging RAM (CBRAM): An Emerging Non-volatile Memory Technology Scalable to Sub 20 nm. *IEDM Tech. Dig.* **2005**, 773–776.
7. Son, J. Y.; Shin, Y.-H.; Kim, H.; Jang, H. M. NiO Resistive Random Access Memory Nanocapacitor Array on Graphene. *ACS Nano* **2010**, *4*, 2655–2658.
8. Lee, M.-J.; Han, S.; Jeon, S. H.; Park, B. H.; Kang, B. S.; Ahn, S.-E.; Kim, K. H.; Lee, C. B.; Kim, C. J.; Yoo, I.-K.; et al. Electrical Manipulation of Nanofilaments in Transition-Metal Oxides for Resistance-Based Memory. *Nano Lett.* **2009**, *9*, 1467–1481.
9. Strukov, D. B.; Snider, G. S.; Stewart, D. R.; Williams, R. S. The Missing Memristor Found. *Nature* **2008**, *453*, 80–83.
10. Jo, S. H.; Kim, K.-H.; Lu, W. Programmable Resistance Switching in Nanoscale Two-Terminal Devices. *Nano Lett.* **2009**, *9*, 469–500.
11. Yang, J. J.; Pickett, M. D.; Li, X.; Ohlberg, D. A. A.; Stewart, D. R.; Williams, R. S. Memristive Switching Mechanism for Metal/Oxide/Metal Nanodevices. *Nat. Nanotechnol.* **2008**, *3*, 429–433.
12. Chua, L. O. Memristor—The Missing Circuit Element. *IEEE Trans. Circuit Theory* **1971**, *18*, 507–519.
13. Borghetti, J.; Snider, G. S.; Kuekes, P. J.; Yang, J. J.; Stewart, D. R.; Williams, R. S. 'Memristive' Switches Enable 'Stateful' Logic Operations *via* Material Implication. *Nature* **2010**, *464*, 873–876.
14. Jo, S. H.; Chang, T.; Ebong, I.; Bhadviya, B. B.; Mazumder, P.; Lu, W. Nanoscale Memristor Device as Synapse in Neuromorphic Systems. *Nano Lett.* **2010**, *10*, 1297–1301.
15. Hasegawa, T.; Ohno, T.; Terabe, K.; Tsuruoka, T.; Nakayama, T.; Gimzewski, J. K.; Aono, M. Learning Abilities Achieved by a Single Solid-State Atomic Switch. *Adv. Mater.* **2010**, *22*, 1831–1834.
16. Russo, U.; Kamalanathan, D.; Ielmini, D.; Lacaita, A. L.; Kozicki, M. N. Study of Multilevel Programming in Programmable Metallization Cell (PMC) Memory. *IEEE Trans. Electron Device Lett.* **2009**, *56*, 1040–1047.
17. Yang, Y. C.; Pan, F.; Liu, Q.; Liu, M.; Zeng, F. Fully Room-Temperature-Fabricated Nonvolatile Resistive Memory for Ultrafast and High-Density Memory Application. *Nano Lett.* **2009**, *9*, 1636–1643.
18. Xu, Z.; Bando, Y.; Wang, W.; Bai, X.; Golberg, D. Real-Time *In Situ* HRTEM-Resolved Resistance Switching of Ag_2S Nanoscale Ionic Conductor. *ACS Nano* **2010**, *4*, 2515–2522.
19. Kim, K.-H.; Jo, S. H.; Gaba, S.; Lu, W. Nanoscale Resistive Memory with Intrinsic Diode Characteristics and Long Endurance. *Appl. Phys. Lett.* **2010**, *96*, 053106.
20. Park, C; Jeon, S. H.; Chae, S. C.; Han, S.; Park, B. H.; Seo, S.; Kim, D.-W. Role of Structural Defects in the Unipolar Resistive Switching Characteristics of Pt/NiO/Pt Structures. *Appl. Phys. Lett.* **2008**, *93*, 042102.
21. Park, J.-W.; Park, J.-W.; Jung, K.; Yang, M. K.; Lee, J.-K. Influence of Oxygen Content on Electrical Properties of NiO Films Grown by RF Reactive Sputtering for Resistive Random-Access Memory Applications. *J. Vac. Sci. Technol. B* **2006**, *24*, 2205–2208.
22. Lin, C.-Y.; Wu, C.-Y.; Wu, C.-Y.; Lee, T.-C.; Yang, F.-L.; Hu, C.; Tseng, T.-Y. Effect of Top Electrode Material on Resistive Switching Properties of ZrO_2 Film Memory Devices. *IEEE Electron Device Lett.* **2007**, *28*, 366–368.
23. Liu, Q.; Long, S.; Wang, W.; Zuo, Q.; Zhang, S.; Chen, J.; Liu, M. Improvement of Resistive Switching Properties in ZrO_2-Based ReRAM with Implanted Ti Ions. *IEEE Electron Device Lett.* **2009**, *30*, 1335–1337.
24. Yoon, J.; Choi, H.; Lee, D.; Park, J.-B.; Lee, J.; Seong, D.-J.; Ju, Y.; Chang, M.; Jung, S.; Hwang, H. Excellent Switching Uniformity of Cu-Doped MnO_x/GdO_x Bilayer for Nonvolatile Memory Applications. *IEEE Electron Device Lett.* **2009**, *30*, 457–459.
25. Liu, Q.; Dou, C.; Wang, Y.; Long, S.; Wang, W.; Liu, M.; Zhang, M.; Chen, J. Formation of Multiple Conductive Filaments in the Cu/ZrO_2:Cu/Pt Device. *Appl. Phys. Lett.* **2009**, *95*, 023501.
26. Schindler, C.; Staikov, G.; Waser, R. Electrode Kinetics of Cu-SiO_2-Based Resistive Switching Cells: Overcoming the Voltage-Time Dilemma of Electrochemical Metallization Memories. *Appl. Phys. Lett.* **2009**, *94*, 072109.
27. Waser, R.; Dittmann, R.; Staikov, G.; Szot, K. Redox-Based Resistive Switching Memories—Nanoionic Mechanisms, Prospects, and Challenges. *Adv. Mater.* **2009**, *21*, 2632–2663.
28. Guo, X.; Schindler, C.; Menzel, S.; Waser, R. Understanding the Switching-Off Mechanism in Ag^+ Migration Based Resistively Switching Model Systems. *Appl. Phys. Lett.* **2007**, *91*, 133513.
29. Guan, W.; Liu, M.; Long, S.; Liu, Q.; Wang, W. On the Resistive Switching Mechanisms of Cu/ZrO_2:Cu/Pt. *Appl. Phys. Lett.* **2008**, *93*, 223506.

30. Wang, Z.; Griffin, P. B.; McVittie, J.; Wong, S.; McIntyre, P. C.; Nishi, Y. Resistive Switching Mechanism in $Zn_xCd_{1-x}S$ Nonvolatile Memory Devices. *IEEE Electron Device Lett.* **2007**, *28*, 14–16.
31. Guan, W.; Long, S.; Liu, Q.; Liu, M.; Wang, W. Nonpolar Nonvolatile Resistive Switching in Cu Doped ZrO_2. *IEEE Electron Device Lett.* **2008**, *29*, 434–437.
32. Guan, W.; Long, S.; Liu, M.; Li, Z.; Hu, Y.; Liu, Q. Fabrication and Charging Characteristics of MOS Capacitor Structure with Metal Nanocrystals Embedded in Gate Oxide. *J. Phys. D: Appl. Phys.* **2007**, *40*, 2754–2758.
33. Yang, J. J.; Strachan, J. P.; Xia, Q. F.; Ohlberg, D. A. A.; Kuekes, P. J.; Kelley, R. D.; Stickle, W. F.; Stewart, D. R.; Medeiros-Ribeiro G.; Willams, R. S. Diffusion of Adhesion Layer Metals Controls Nanoscale Memristive Switching. *Adv. Mater.* In press.